Journal of
Plankton Research

plankt.oxfordjournals.org

J. Plankton Res. (2016) 38(2): 167–182. First published online December 17, 2015 doi:10.1093/plankt/fbv103

Costa Rica Dome: Flux and Zinc Experiments

Plankton dynamics and biogeochemical fluxes in the Costa Rica Dome: introduction to the CRD Flux and Zinc Experiments

MICHAEL R. LANDRY[1]*, ALAIN DE VERNEIL[1], JOAQUIM I. GOES[2] AND JAMES W. MOFFETT[3]

[1]SCRIPPS INSTITUTION OF OCEANOGRAPHY, UNIVERSITY OF CALIFORNIA AT SAN DIEGO, 9500 GILMAN DR., LA JOLLA, CA 92093-0227, USA, [2]DEPARTMENT OF MARINE BIOLOGY AND PALEOENVIRONMENT, LAMONT DOHERTY EARTH OBSERVATORY AT COLUMBIA UNIVERSITY, PALISADES, NY 10964, USA AND [3]DEPARTMENT OF BIOLOGICAL SCIENCES, UNIVERSITY OF SOUTHERN CALIFORNIA, LOS ANGELES, CA 90089, USA

*CORRESPONDING AUTHOR: mlandry@ucsd.edu

Received April 26, 2015; accepted November 9, 2015

Corresponding editor: Roger Harris

The Costa Rica Dome (CRD) is an open-ocean upwelling system in the Eastern Tropical Pacific that overlies the ocean's largest oxygen minimum zone (OMZ). The region has unique characteristics, biomass dominance by picophytoplankton, suppressed diatoms, high biomass of higher consumers and presumptive trace metal limitation, but is poorly understood in terms of pelagic stock and process relationships, including productivity and production controls. Here, we describe the goals, project design, physical context and major findings of the Flux and Zinc Experiments cruise conducted in June–July 2010 to assess trophic flux relationships and elemental controls on phytoplankton in the CRD. Despite sampling during a year of suppressed summertime surface chlorophyll, cruise results show high productivity ($\sim$1 g C m^{-2} day^{-1}), high new production relative to export, balanced production and grazing, disproportionate biomass-specific productivity of large phytoplankton and high zooplankton stocks. Zinc concentrations are low in surface waters relative to phosphorous and silicate in other regions, providing conditions conducive to picophytoplankton, like *Synechococcus*, with low Zn requirements. Experiments nonetheless highlight phytoplankton limitation or co-limitation by silicic acid, driven by a strong silica pump that is linked to low dissolution of biogenic silica in the cold shallow thermocline of the lower euphotic zone.

KEYWORDS: trophic; community; structure; limitation; food web

available online at www.plankt.oxfordjournals.org

INTRODUCTION

This issue contains papers from a multidisciplinary study of upper-ocean plankton ecology and surface to mid-water biogeochemistry of the Costa Rica Dome (CRD), conducted on cruise MV1008 of *R/V Melville* from 22 June to 25 July 2010. The study, funded by the US National Science Foundation (NSF), was initially designed to test two hypothesized mechanisms of phytoplankton bloom regulation in the Arabian Sea: grazer control (Smith, 2001; Goericke, 2002) and iron limitation (Wiggert *et al.*, 2006; Naqvi *et al.*, 2010). However, just prior to what would have been the original scheduled cruise for that project (July 2009), piracy concerns in the northwestern Indian Ocean closed the area to scientific research, a situation that continues now 6 years later. After some deliberation and with NSF approval, the project was recast for the CRD region in the Eastern Tropical Pacific (ETP). The CRD has certain similarities to the Arabian Sea, such as an upwelling center, an oxygen minimum zone (OMZ) of global significance and the presumptive limitation of phytoplankton by a trace element. CRD research also fit the strengths and interests of our group, as well as the working areas of major US research vessels in summer 2010.

In planning our cruise, we found that the CRD was well described physically, including its circulation, seasonal development and decay (Fiedler, 2002; Fiedler and Talley, 2006; Kessler, 2006). However, it was poorly characterized in terms of lower food-web trophic processes, carbon cycling from production to export, basic standing stock and rate relationships and phytoplankton regulatory mechanisms. In the late 1960s, the EASTROPAC Program conducted seasonal surveys of the ETP over an 18-month period, providing the first comprehensive measurements of plankton stocks and distributions in the region (Love, 1972–1978; https://swfsc.noaa.gov/eastropac-atlas/). Some of the insights from that program anticipated what are now generally accepted cornerstones of modern understanding of open-ocean pelagic ecology, for example, the close coupling of primary production and zooplankton grazing (Longhurst, 1976) and the dominant grazing role of microzooplankton (Beers and Stewart, 1971). However, they were made solely from considerations of biomass relationships, with no measurements of the actual processes. We found also that understanding of primary production processes in the CRD region was equivocal at best. EASTROPAC results (Owen and Zeitzschel, 1970) as well as modern shipboard measurements (Pennington *et al.*, 2006) both point to relatively modest production values <400 mg C m^{-2} day^{-1}; in contrast, modeled production estimates for the region are two to three times higher (Pennington *et al.*, 2006). Thus, appropriate measurements and analyses to resolve food-web fluxes, from production to grazing and export, became a central theme of our CRD research agenda.

Recent cruises in the CRD had also highlighted unique properties of the region that relate to its trophic structure and potential regulatory mechanisms. These observations confirmed early reports of very high abundances of picophytoplankton, dominated by the photosynthetic bacterium *Synechococcus* (SYN) at concentrations exceeding 10^6 mL^{-1} (Li *et al.*, 1983; Saito *et al.*, 2005). They also provided preliminary evidence that trace elements other than iron (Fe) might limit or co-limit phytoplankton community structure and productivity in the CRD, as might be expected from the very different assemblages, dominated by *Prochlorococcus* (PRO) with much lower SYN abundances (10^4 mL^{-1}) that occur in Fe-limited waters of the eastern equatorial Pacific (Landry and Kirchman, 2002). In an experiment conducted in the CRD on a cruise in August 2000, Franck *et al.* (Franck *et al.*, 2003) demonstrated that small pennate diatoms responded strongly to zinc (Zn) added in combination with Fe, compared with Fe addition alone. In other results from the same cruise, Saito *et al.* (Saito *et al.*, 2005) found that strong binding ligands for cobalt (Co), believed to be produced by SYN to satisfy its high Co requirement, deplete labile Co bioavailability to other phytoplankton. Cobalt is, however, mainly useful to eukaryote taxa like diatoms as a substitute for Zn. In addition, because Zn requirements for cyanobacteria are low compared with those for eukaryotic phytoplankton (Saito *et al.*, 2003), we focused on Zn as a possibly limiting or co-limiting micronutrient (in combination with Fe or Si) that would be consistent with both the extraordinary high concentrations of SYN in the region and the suppression of their larger eukaryotic competitors, like diatoms. We also hypothesized that low Zn concentrations in SYN cells could affect growth or grazing responses of their eukaryote protistan consumers, thereby potentially interfering with efficient grazer control of the SYN population and picophytoplankton generally, the expected role of small protistan grazers in trace metal limited systems (Landry *et al.*, 1997, 2000, and references therein). The hypothesized effects of Zn limitation, promoting growth of SYN over larger eukaryote competitors while diminishing grazing pressure on SYN, were thus among the ideas to be tested in our research cruise to the CRD.

The project name FLUx and Zinc Experiments (FLUZiE) emphasizes the two main cruise goals: (i) to quantify processes and assess flux relationships within and out of the CRD euphotic zone, and (ii) to evaluate grazing and trace metal/nutrient controls on primary production and phytoplankton standing stocks, with a focus on Zn. Additional collaborators and components

were added to complement these objectives, and also to take advantage of the opportunity to measure biogeochemical cycling and microbial populations in underlying OMZ waters at the same time that upper water-column processes were being investigated. The Cruise Report and data archives are available at http://www.bco-dmo.org/project/515387. Here, we provide a general overview of the study site and project design, the prevailing environmental conditions of the CRD during summer 2010, the physical context for sampling and experimental studies and a brief overview of the scientific findings from the expedition.

STUDY AREA

Seasonal evolution of the Costa Rica Dome

The CRD is a recurrent seasonal phenomenon of the ETP that results as a consequence of winds, currents and the presence of the Central American landmass. The CRD occurs at the eastern terminus of a thermocline ridge, associated with both the North Equatorial Counter Current (NECC) on the southern slope and the North Equatorial Current on the northern slope, both in geostrophic balance. The result is a thermal dome centered near 9°N, 90°W during summer months (Fiedler, 2002).

The physical drivers of the CRD have been a subject of historical debate. Wyrtki (Wyrtki, 1964) originally proposed that the upwelling was due to the geostrophic deflection of the NECC, and he used a heat budget model to calculate an upwelling rate, though for wintertime conditions when the CRD is actively weakening according to contemporary theory. Hoffman *et al.* (Hofmann *et al.*, 1981) argued that local wind stress curl generates CRD upwelling, which then weakens over winter causing the CRD to propagate westward as a Rossby wave. The numerical modeling study of Umatani and Yamagata (Umatani and Yamagata, 1991), however, found that summertime wind stress curl was relatively weak and not co-located with the CRD. They made the case that the annual cycle of strong NE Trade Winds blowing through topographic gaps at the Gulf of Papagayo, as well as Tehuantepec and Panama, during the wintertime followed by SE Trade Winds over the open ocean from late spring into fall were both necessary for the evolution of the CRD. That explanation, echoed by Fiedler (Fiedler, 2002), gives an annual cycle in which the NE Trades create an embryonic dome near the Central American coast that moves offshore, where it matures under the influence of the summertime SE Trades and the strengthening NECC associated with the northward migration of the InterTropical Convergence Zone (ITCZ). The CRD moves westward and deepens during the winter, when a new CRD is created at the coast.

In Fig. 1, we use monthly mean values of absolute dynamic topography (ADT) from AVISO satellite

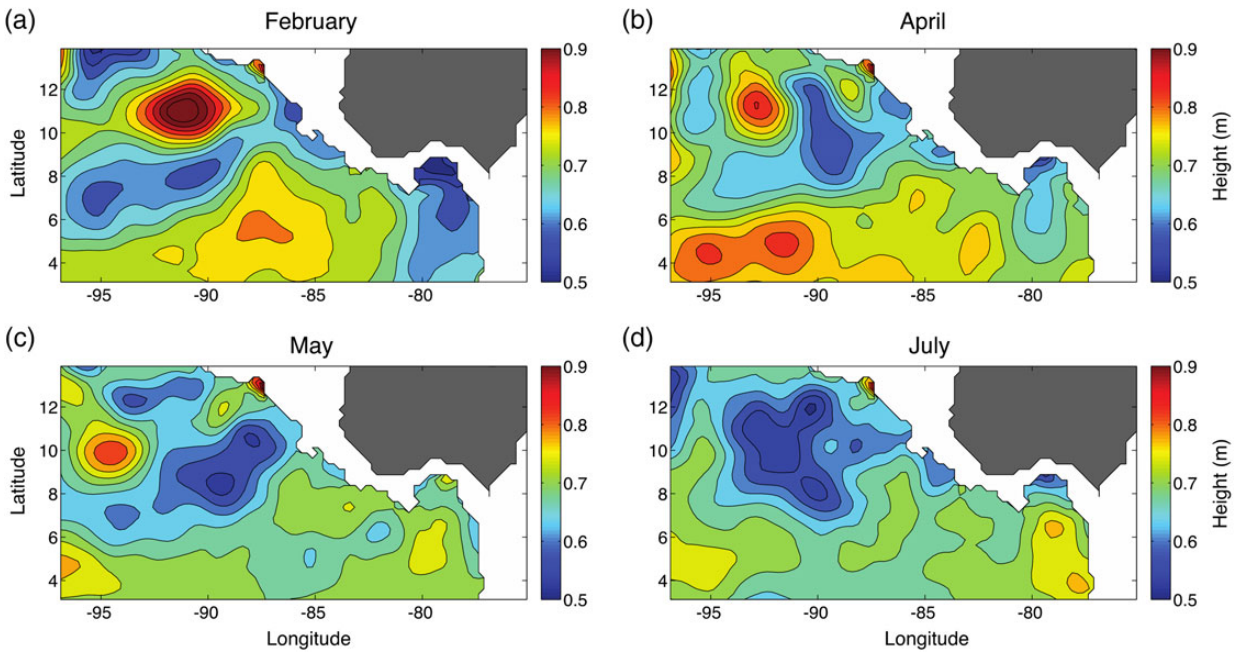

Fig. 1. Mean monthly images of satellite-derived absolute dynamic topography (ADT). Central America, from Mexico to northern South America is shown in white. (**a**) February ADT, showing both cyclonic (low ADT) and anti-cyclonic (high ADT) features near the coast. (**b** and **c**) April and May, where anti-cyclonic features continue to move offshore while a low forms offshore. (**d**) July, when the CRD is clearly visible.

altimetry (http://www.aviso.altimetry.fr/duacs/) to show seasonal evolution preceding the cruise in July 2010. The general pattern is consistent with previous results (Umatani and Yamagata, 1991; Fiedler, 2002). Though sometimes not visible in the monthly mean data, both anti-cyclonic (higher height values) and cyclonic features (lower height values) propagated from the coast from February through April, presumably due to NE Trades forcing. Around May/June, a persistent feature with reduced (cyclonic) height developed in the region, though centered somewhat northwest of 9°N, 90°W. This region of low dynamic height was consistent with the CRD.

ETP conditions in summer 2010

In satellite summertime composites of sea surface Chl *a* from 2003 to 2014 (Supplementary Data, Fig. S1), summer 2010 stands out as an unusual year in terms of cloud cover (more flagged pixels than any of the 12 summers analyzed), and it shows a relatively low-surface Chl *a* expression in the CRD region relative to adjacent waters. According to the Ocean Niño Index (ONI) for January–March 2010 was classified as a moderate El Niño year in the ETP, which is indicative of ocean conditions leading up to the cruise (Fig. 2). However, during the cruise itself, the ONI is seen to be relatively neutral and shifting rapidly to La Niña conditions (Fig. 2). Consistent with the timing of this shift, wintertime sea surface temperatures were anomalously warm in the region preceding the cruise, but not unusually so during the summer and later half of the year (Fig. 3). Nonetheless, the Chl *a* expression of the CRD region was severely suppressed throughout 2010. In a decade of satellite images analyzed from 2004 to 2014, 2010 is the only year without a clear mid-summer elevation of surface Chl *a*, and it is markedly depressed relative to regionally averaged mid-summer Chl *a* values for adjacent years 2009 and 2011 and especially relative to the massive bloom concentrations seen in 2013 (Fig. 3).

SAMPLING AND EXPERIMENTAL PROGRAM

The locations of the two main elements of the cruise plan, semi-Lagrangian experimental cycles and a sampling transect, are shown in Fig. 4. The dates and beginning geographic coordinates for the major cruise operations are given in Table I.

After leaving port in Puntarenas, Costa Rica, we first undertook an initial experimental study (Cycle 1) in waters close to the coast, since we had to return to port within a few days to pick up a shipment of ^{14}C bicarbonate delayed in customs (primary production measurements were not made during Cycle 1). After the transfer, we transited to 6.6°N, 88.5°W to begin a sampling transect to 10°N, 92°W, crossing the expected central dome area of the CRD. That area, characterized by a shallow thermocline, was sampled more intensively over an additional day and a half, during which five WMO surface drifters with shallow mixed-layer drogues (World Meteorological Organization, Global Drifter Program) were deployed at various locations to assess currents and dispersion patterns. Experimental Cycle 2 was conducted in the vicinity of the dome center, and at the end of that experiment a final WMO drifter was released to relocate that water for later study in Cycle 4. Meanwhile, a third experiment (Cycle 3) was conducted on the outer northwest edge of the dome region. Returning to the central dome region, we conducted Cycle 4 in the vicinity of the WMO drifter. The last experiment (Cycle 5) was done to the east of the dome center heading back to the coast in the rapidly moving NECC.

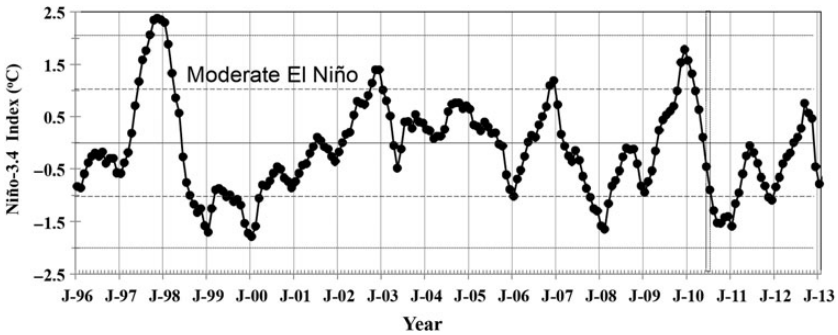

Fig. 2. Time-series variability of Ocean Niño Index (ONI) for characterizing El-Niño and La-Niña years in the tropical Pacific Ocean. Updated ONI data are from http://www.cpc.ncep.noaa.gov/products/analysis_monitoring/ensostuff/ensoyears.shtml. ONI is the running 3-month mean of SST anomaly for the Niño 3.4 region (5°N–5°S, 120–170°W) accounting for global warming since 1950. 2010 was classified as a moderate El Niño year based on having positive temperature anomalies between +1.0 and 1.4°C for at least three consecutive overlapping 3 months. Bar in mid-2010 indicates cruise period.

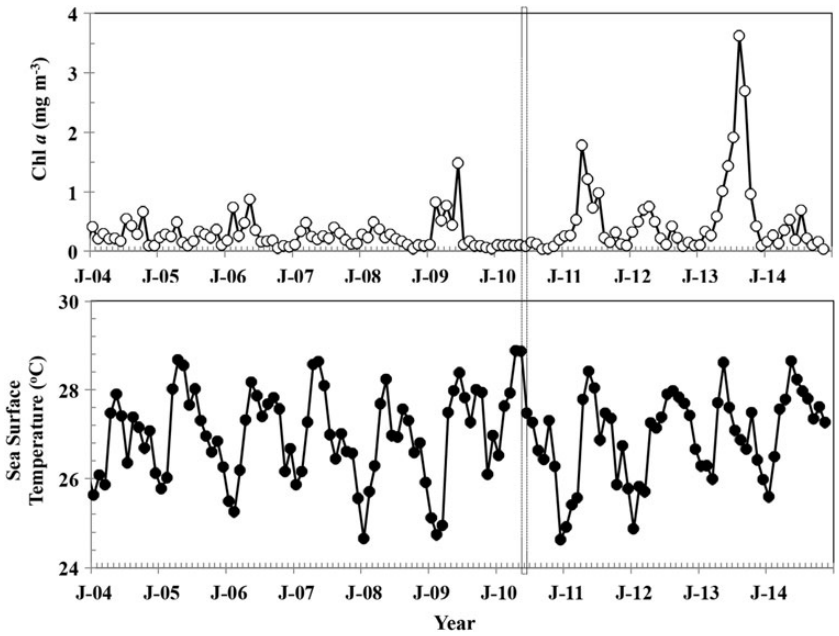

Fig. 3. Area-averaged values of sea surface temperature (°C) and chlorophyll *a* (mg m^{-3}) in the Costa Rica Dome region of the Eastern Tropical Pacific from 2004 to 2014. Monthly averaged data for the area of 8−11°N, 88−93°W were derived from MODIS-Aqua as 4-km SMI images extracted using NASA's Giovanni, interactive Visualization and Analysis. Yearly tic marks begin in January (J). All flagged pixels were excluded from the analysis. Horizontal bar indicates cruise period, 22 June−25 July 2010.

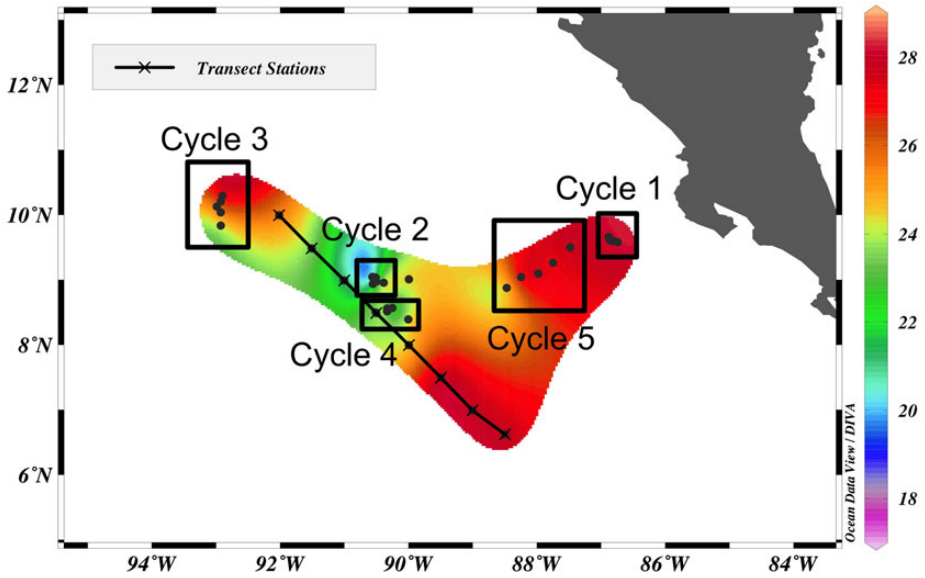

Fig. 4. Cruise study area in the CRD, 22 June−25 July 2010. Transect is shown by line with marks for sampling locations. Experimental cycles are shown in boxes; each point marks location of daily morning sampling and *in situ* incubation experiment. Temperature scale is temperature at 20-m depth; cool water denotes proximity to central dome region.

At each transect sampling station, we lowered a fast repetition rate fluorometer to 100 m. That was followed by zooplankton net collections (200-μm mesh, 1-m^2 ring net) with an oblique tow to ∼150-m depth. The water was then sampled to 500 m with a Conductivity-Temperature-Depth (CTD) rosette system (hydrography, nutrients and phytoplankton), and a second hydrocast was made with TM-clean rosette to collect samples for trace metal analyses.

During the majority of the cruise period, we conducted the five "cycle" experiments of typically 4-day duration (3 days for Cycle 1) following the paths of a

Table I: Dates and locations of experimental cycles, transect sampling and WMO drifter deployments in the CRD during June–July 2010

Dates	Lat (°N)	Lon (°W)	Operation
23–27 June	9.715	87.004	Cycle 1 experiments
29 June	6.628	88.497	Begin transect survey
1 July	10.000	92.000	End transect survey
2–3 July			Sampling in central dome area
3 July	9.000	90.127	WMO drifter 43533 deployed (#1)
3 July	9.000	90.904	WMO drifter 43535 deployed (#2)
3 July	9.038	90.551	WMO drifter 43536 deployed (#3)
3 July	9.037	90.573	WMO drifter 43537 deployed (#4)
3 July	9.051	90.564	WMO drifter 43540 deployed (#5)
4–8 July	9.037	90.564	Cycle 2 experiments
8 July	8.924	90.316	WMO drifter 43541 deployed (#6)
9–13 July	10.416	92.916	Cycle 3 experiments
15–19 July	8.546	90.399	Cycle 4 experiments
20–24 July	8.877	88.465	Cycle 5 experiments

Locations for cycle experiments denote initial positions of the experiments, marked by deployment of the sediment trap drift array; daily sampling points are shown in Fig. 4. Beginning and endpoints for transect sampling are as depicted in Fig. 4. Drifter deployments give 5-digit WMO identifier number (World Meteorological Organization, Global Drifter Program), as well as informal #1–6 numbers for drifter tracks in Fig. 8. Dates are local time, beginning at mid-night for cycle sediment trap deployments.

satellite-tracked surface drifter with a holey sock drogue centered at 15 m (Landry *et al.*, 2009). Each of these experiments involved a coordinated series of *in situ* sampling and experiments as well as shipboard experimental activities to measure changes in hydrography and the plankton community in the tracked water parcel, to determine process rates (production, growth and grazing) in incubation experiments and to evaluate nutrient and trace metal limitation of the phytoplankton community. Export was assessed by the 234-Thorium disequilibrium method and by measured fluxes into sediment traps deployed below the euphotic zone at 90–100 m on a second drifter array (deployed at the start of the cycle and recovered at the end). Process experiments were conducted daily using water collected on a pre-dawn CTD hydrocast at eight depths from the top to the bottom of the euphotic zone. Bottle experiments for ^{14}C-primary production, nitrate uptake, net biogenic silica incorporation and phytoplankton growth and microzooplankton grazing rates (dilution) were incubated under *in situ* conditions of temperature and light in net bags attached at the depth of collection to a wire hanging below the drifter. Net tow samples were collected daily at mid-day and mid-night for biomass and grazing assessments (gut fluorescence) of mesozooplankton in the upper 150 m, and stratified net sampling for mesozooplankton and micronekton (1-m^2 MOCNESS) was done at 1000 m at least once each during daytime and nighttime hours on each cycle. Multiple casts were made with the trace metal rosette during each cycle to sample for depth distributions of trace metal (Fe, Zn) concentrations and to set up shipboard experiments to test for limitation of various treatment combinations of added Fe, Zn and Si. Additional CTD sampling was done in the OMZ to study nitrogen sources and sinks and to collect samples for molecular characterization of the microbial community

PHYSICAL CONTEXT FOR SAMPLING AND EXPERIMENTS

Transect and cycle hydrography

The mean satellite ADT for the transect indicates that sampling began outside of the low height region, which was then entered with Stations 2 and 3 on the periphery. Temperature profiles along the transect show isotherm shoaling consistent with the CRD (Fig. 5b). Temperature is colored to highlight the 24°C isotherm emphasized in Wyrtki (Wyrtki, 1964). That isotherm did not reach <10 m as reported by Wyrtki, though this may be due to his wintertime sampling or to weakened upwelling conditions in 2010. However, the isotherm shoals by approximately 15 m, and is shallowest between Stations (CTD casts) 4 and 6, co-located with a maximum in CTD fluorescence (Fig. 5c). Satellite topography suggests that sampling Stations 7 and 8 were also within the dome. Wyrtki's (Wyrtki, 1964) figures of the CRD suggest patchiness in both tracers and inferred upwelling, and this view is consistent with the irregular shape of the CRD feature as visualized by satellite ADT.

Mean temperature profiles for the five cycles reflect similar trends as the transect sampling (Fig. 6a). Cycles 1 and 5, nearest to the coast, show depressed thermoclines, with the 24°C isotherm at ~34 m. In contrast, Cycles 2 and 4, in the central dome area, show the isotherm at ~24 m. Cycles 2 and 4 also meet Fiedler's criterion for being considered in the dome area, with the 20°C isotherm above 35 m depth (Fiedler, 2001). By this definition, Cycle 3 is on the outer margin of the dome, which agrees with its peripheral position in satellite ADT (Fig. 6c), and Cycles 1 and 5 are clearly out of the dome. Temperature–salinity relationships from these five cycles, however, suggest slightly different spatial relationships. While Cycle 5 had a depressed thermocline, similar to Cycle 1, its T–S signature near the surface most closely resembles that of Cycle 4 (Fig. 6b). This suggests that while the dynamical context for this cycle has changed (now outside the dome with a depressed thermocline), the surface waters from Cycle 5 may ultimately have derived from the Cycle 4 vicinity, considered in the dome. The possible entrainment of water associated with the CRD

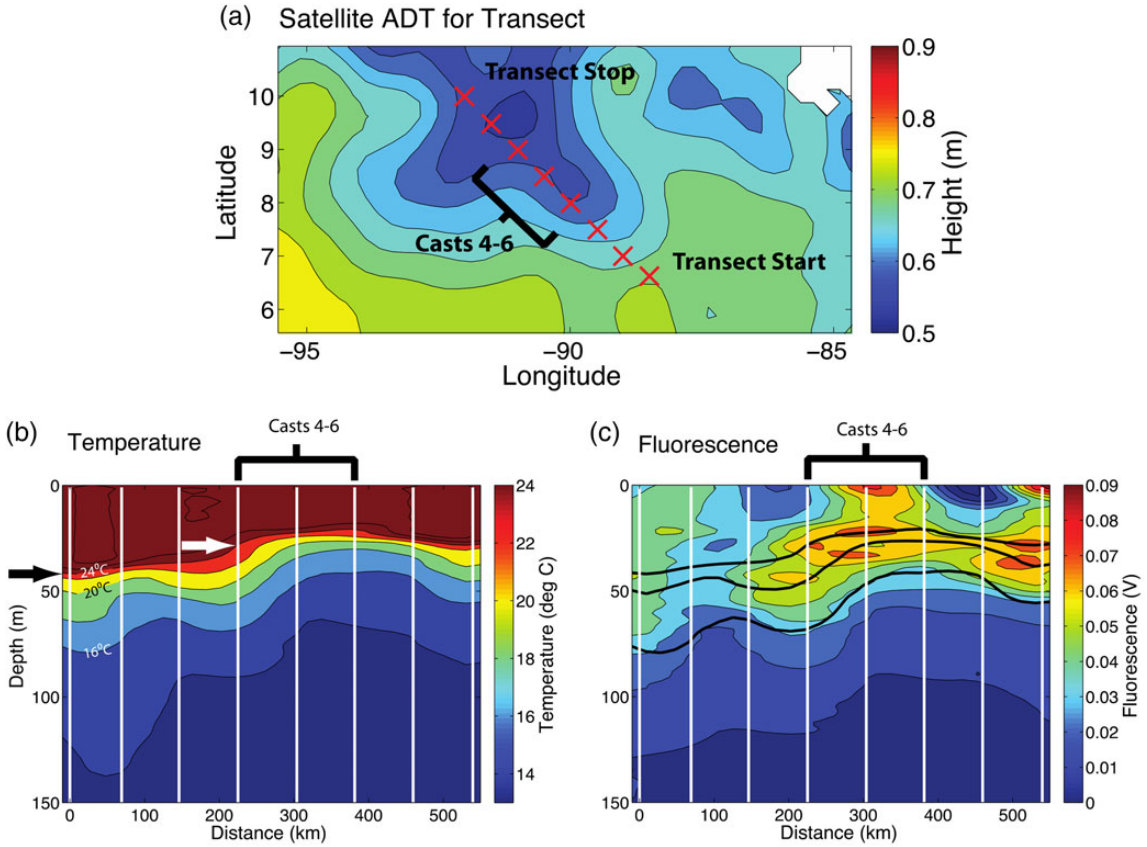

Fig. 5. Hydrographic conditions during CRD transect sampling, 29 June–3 July 2010. (**a**) Satellite ADT during the transect, with CTD cast locations depicted as crosses. (**b**) Objective map of temperature isotherms, with arrows depicting locations of 24°C isotherm outside and inside the dome. Vertical lines are cast locations. (**c**) CTD Chl *a* fluorescence. Vertical lines depict cast locations, 16, 20 and 24°C isotherm lines from (b) included.

toward the coastal region implies that the enhanced biological production associated with the CRD may not all remain local.

Surface current flows during experimental cycles

While extensive cloud cover in summer 2010 precluded good images of satellite sea surface temperature and Chl *a* during the cruise, both dynamic topography (ADT = SSH, reflecting large-scale variations in water-column structure and geostrophic circulation) and sea-level anomalies (SLA, reflecting deviations in SSH caused by transient mesoscale processes such as eddies) were available from daily AVISO analyses, along with inferred geostrophic currents. Both geostrophic velocity datasets were linearly interpolated and compared for daily intervals to currents measured from the shipboard Acoustic Doppler Current Profiler (ADCP) bin nearest to the surface (29 m). The ADCP measurements are 5-min ensembles produced by UHDAS (Firing and Hummon, 2010). Despite qualitative large-scale differences in ADT and SLA, the daily vector correlations (as defined by Crosby *et al.*, 1993) from both datasets were similar, with the average correlation being 0.562 and 0.556 (out of a range from 0 to 2) for ADT and SLA, respectively. Since the CRD is a recurrent regional feature, here we used ADT because it includes the long-term CRD contribution to dynamic height, whereas SLA does not.

Figure 8 shows the positions of drift array deployments during the five cycles, and the average ADT and inferred currents. The inset in each figure is the regional ADT for each cycle, which varied over the 35 days of the cruise. Cycle 1, located near the coast, shows the drift array going southeast, consistent with ADT at that time. The regional view of ADT during Cycle 1 suggests that this southeast flow is associated with a deflection of the eastern low height CRD boundary (Fig. 7a), and is possibly a continuation of the NECC, which flows south of the CRD.

Cycle 2 is near the shoaled isotherms and high-fluorescence area identified during transect sampling. Drift array tracks in this location were very complex, with

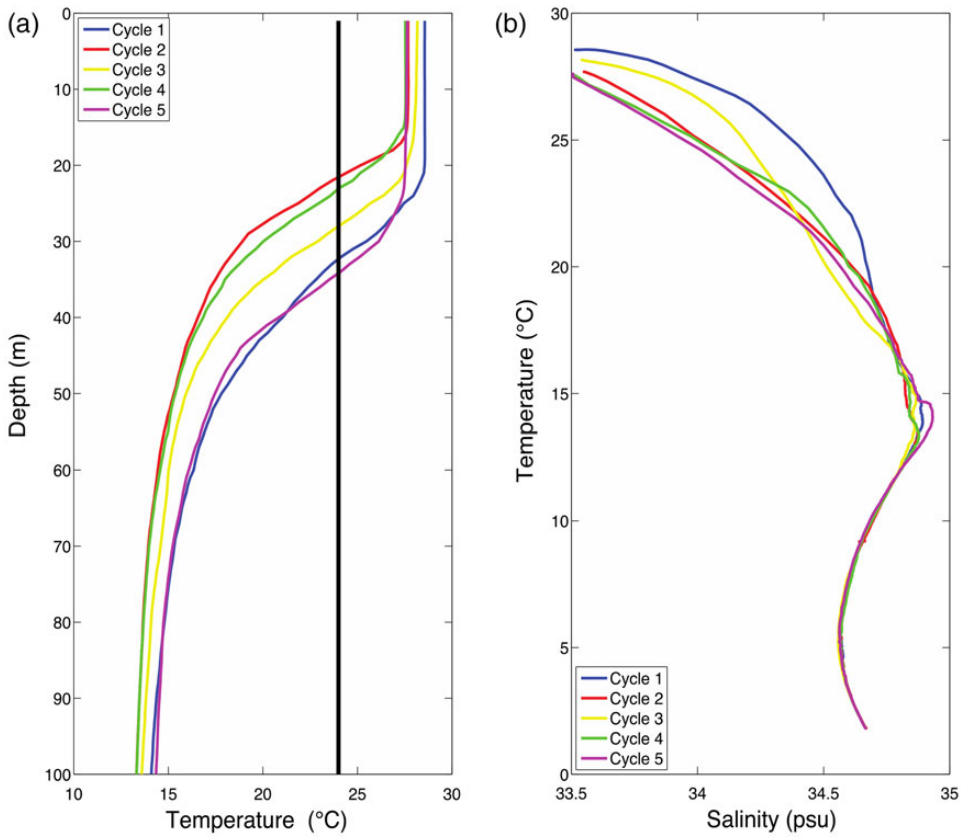

Fig. 6. Cruise averages of (**a**) temperature profiles and (**b**) temperature–salinity relationships for experimental Cycles 1–5. 24°C line is shown for reference.

spiraling flow of significant amplitude due to strong inertial tides and a little net southeastward displacement. Satellite inferences of current velocities are also complicated in this region, showing a convergence to the north of the drift array, and a larger cyclonic recirculation around a lobe of low height to the south (Fig. 7b). The $\frac{1}{4}$-degree resolution provided by AVISO is somewhat coarse, and ADCP data for this cycle show varying currents with no mean direction, suggesting a quiescent region with lower-order dynamical effects.

Cycle 3, located to the northwest of Cycle 2, is on the western periphery of the CRD as identified by satellite (Fig. 7c). The constant southern trajectory of the drift array is consistent with satellite velocity patterns. As mentioned previously, its intermediate temperature profile suggests the influence of the CRD. However, its T–S signature near the surface is intermediate, more similar to Cycle 1 than the other three.

The drifter array track for Cycle 4 resembles that for Cycle 2 in location, complex satellite velocities and intermittent southeastern direction (Fig. 7d). With similar drift array tracks, satellite currents, temperature profiles and T–S signatures, Cycles 2 and 4 appear to be most similar from a physical standpoint, which is consistent with our intention to have Cycle 4 to be a follow-on experiment to surface waters that originally came from the vicinity of Cycle 2.

The coastward movement in Cycle 5 is similar to satellite velocities, which indicate a shift in the direction of water flowing south of the CRD (Fig. 7e). As mentioned previously, the temperature profile from Cycle 5 reflects that of Cycle 1, suggesting a comparable dynamical situation outside the CRD. However, the T–S relationship for the mixed layer in Cycle 5 shows similarities to water from Cycles 2 and 4.

Surface drifter movements

During experimental Cycle 2, six WMO surface drifters (World Meteorological Organization, Global Drifter Program) were deployed to identify water circulation in the vicinity of the CRD. There were originally seven deployed, but one failed to report positions, and one drifter (#5) was taken by a local fishing vessel within a few days of

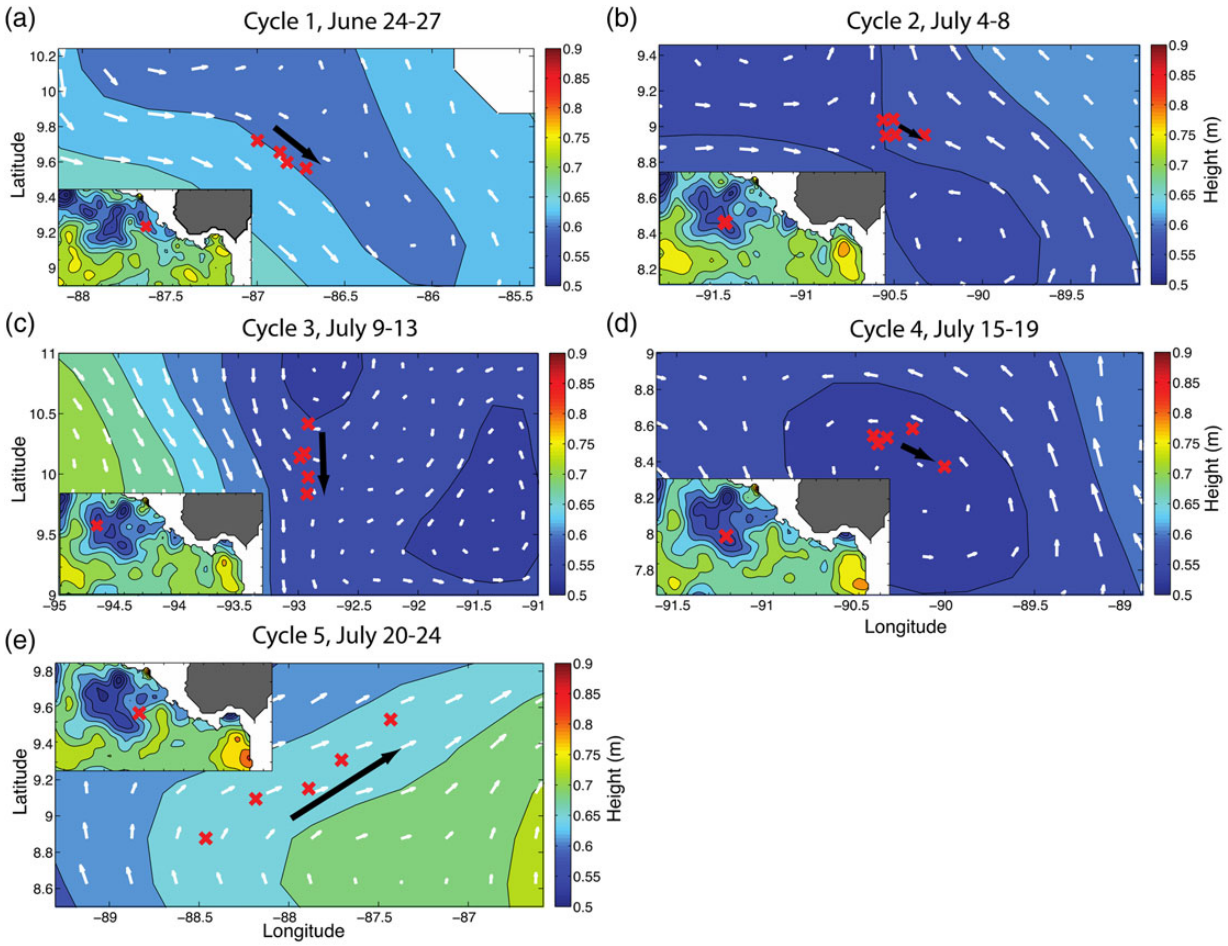

Fig. 7. Locations of early morning CTD casts (X) superimposed on averaged satellite ADT and inferred geostrophic current velocities for experimental Cycles 1–5 (panels **a**–**e**, respectively).

deployment. Fig. 8a shows the six reliable drifter trajectories, along with the mean satellite ADT and velocities for the time period of 6–20 July.

Initially, all the drifters moved in anti-cyclonic orbits suggestive of inertial oscillations. At 9°N latitude, the observed radius of motion, at $\sim\frac{1}{8}$ degree or $\sim$14 km, reflects an estimated mean current velocity of 0.30 m s^{-1} (Gill, 1982). Subsequently, three drifters (#1, 3 and 4) deployed slightly to the north and east of the start of Cycle 2 stopped their inertial oscillations and drifted together to the north. In contrast, the other two drifters (#2 was deployed the furthest to the west, and #6 was released at the end of Cycle 2) remained south, continuing inertial oscillations.

Figure 8b depicts relative dispersion, a metric of particle spread (LaCasce, 2008) calculated from the locations of these drifters, binned over all drifters and the two subsets of drifters. While not sufficient to calculate statistically robust values of vertical diffusivity, the total and subset relative dispersions imply the existence of a branching point in the velocity field where the two subsets separated. The dispersion of both subsets remained relatively constant whereas the overall dispersion increased, reflecting the in-group coherence and between-group separation of the drifters. The different behaviors of these two drifter subsets suggest a complicated mesoscale flow in the vicinity of Cycles 2 and 4. Some water parcels remained in the area, whereas others nearby were entrained into a large-scale current. For reference, the starting positions of Drifters 2 and 3 were 24 km apart, and the two subsequently were taken in very different directions. The last drifter (#6), deployed 20 km from drifter #2′s original position, stayed in that same area.

The O(10-km) scale sensitivity of drifter displacement reflects the horizontal variability present in this region, and the potential influence of (sub)mesoscale flows in determining distributions of biological communities. The

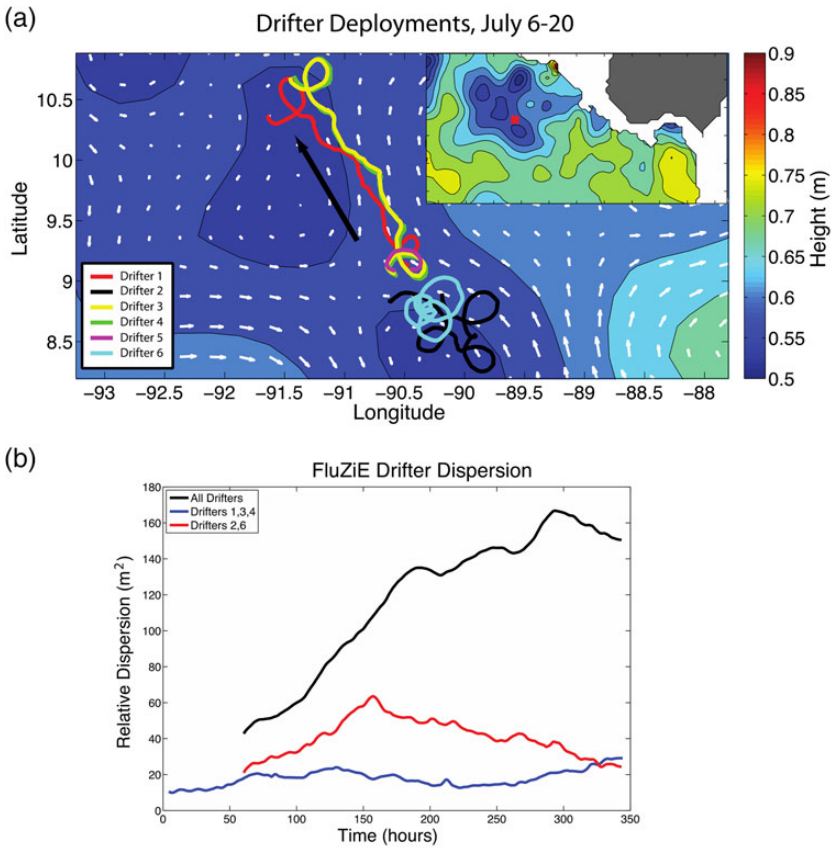

Fig. 8. Trajectories and dispersion of drogued drifters released in vicinity of start of Cycle 2 on 4 July 2010 (marked by X in panel a insert). (**a**) Drifter trajectories, mean satellite ADT and geostrophic velocities. Note inertial tide effects, especially for Drifters 2 and 6. (**b**) Relative dispersion for all drifters, and for drifter subsets 1, 3 and 4 and Drifters 2 and 6.

separation of the drifters, and the hydrographic similarity of Cycle 5 to Cycles 2 and 4, provide the strongest evidence that water associated with the CRD is not statically trapped within the CRD feature, as it occurs with mesoscale eddies that can effectively separate biological assemblages and possibly promote coexistence of diverse phytoplankton groups (d'Ovidio *et al.*, 2010).

OVERVIEW OF MAJOR RESULTS

For the purpose of this introduction, we divide the results of our investigation into three broad themes that fallout from the original cruise goals: (i) plankton dynamics and flux relationships for the CRD euphotic zone; (ii) controls on phytoplankton stocks and production; and (iii) ecology and biogeochemistry of the OMZ. Under each theme, we first provide a brief overview of the components of the project that relate to the theme, then give a bullet-point summary of the key results. Most of the discussion relates to papers that are published together in this issue. However, we also summarize relevant additional products from the cruise that are published elsewhere.

Plankton dynamics and flux relationships

The FLUZiE cruise differed from previous studies of CRD in taking a system-level, process-oriented approach involving a suite of complementary measurements of phytoplankton and zooplankton community biomass, composition and process rates over the full depth range of the euphotic zone and at several locations, in and out of the central dome region. These data consequently provide the first depth-integrated assessments of phytoplankton group-specific contributions to carbon standing stocks, productivity and grazing in the region, as well as the first site-integrated assessments of primary production, new production, net biogenic silica production and export. Taylor *et al.* (Taylor *et al.*, 2016) give details of the community biomass, size structure, composition, depth distribution and spatial variability of phytoplankton based on complementary analyses by microscopy, flow cytometry

and high pressure liquid chromatography pigments. Freibott *et al.* (Freibott *et al.*, 2016) contribute analyses of biomass, community structure and spatial variability of the heterotrophic components of microbial food webs, protistan grazers and bacteria. Gutiérrez-Rodríguez *et al.* (Gutiérrez-Rodríguez *et al.*, 2014) document the spatial variability of picocyanobacterial community structure across the upwelling dome using clone libraries of the *rpoC1* gene and quantitative polymerase chain reaction assays to assess the distributions of genetically distinct SYN and PRO populations. Selph *et al.* (Selph *et al.*, 2016) present estimates of primary productivity and phytoplankton growth rates from standard ^{14}C-uptake and from daily *in situ* incubations of dilution experiments at eight depths in the euphotic zone, analyzed by flow cytometry and pigments for community and group-specific rates. Krause *et al.* (Krause *et al.*, 2016) report the net rates of biogenic silica ($bSiO_2$) production and export, from which they estimate the diatom contribution to new production and organic matter export. Stukel *et al.* (Stukel *et al.*, 2016) measure new production by ^{15}N-nitrate uptake and organic matter export by the ^{234}Th-disequilibrium method and by sediment traps (C, N and P), from which they assess the efficiency of the biological pump. Décima *et al.* (Décima *et al.*, 2016) provide euphotic-zone-integrated estimates of mesozooplankton size-fractioned biomass and grazing impact on phytoplankton. Jackson and Smith (Jackson and Smith, 2016) assessed day–night depth distributions of five co-occurring copepod species of the Eucalanidae family in and out of the central dome region. Landry *et al.* (Landry *et al.*, 2016) combine various process measurements into a community-level synthesis addressing the balance of production and grazing processes, including the contributions of different phytoplankton and grazer groups to carbon-based fluxes. Significant results from this portion of the study include the following:

- Autotroph carbon ranged from 0.7 to 2.4 g C m^{-2}, with higher values in the dome center (Taylor *et al.*, 2016). Pico-sized cells, notably SYN, accounted for >50% of biomass, and more so in the central region. Dinoflagellates dominated the assemblage of larger phytoplankton, with diatoms accounting for 2% or less of biomass throughout the region.
- Assessments of micro-heterotrophs indicate a well-developed microbial food web (Freibott *et al.*, 2016). Heterotrophic dinoflagellates (H-Dino) and nano-sized cells dominated the micro-grazer assemblage. Carbon-based grazing rates were significantly correlated with grazer biomass, and indicated grazer growth rates comparable to those of phytoplankton. Bacterial biomass was significantly correlated with autotrophic carbon and productivity.
- Phylogenetic analysis revealed high picocyanobacterial diversity that included novel SYN and PRO genotypes (Gutiérrez-Rodríguez *et al.*, 2014). Genetically different populations exhibited strong vertical and horizontal spatial partitioning associated with sharp physicochemical gradients. Three SYN genotypes showed fine-scale depth structure in the upper 30–40 m at the dome.
- In contrast to biomass, mixed-layer growth rates of phytoplankton were lowest in the dome center and higher on the edges (Selph *et al.*, 2016). Growth rates of PRO and SYN were balanced by microzooplankton grazing, whereas eukaryotic phytoplankton showed positive net growth. Mean growth rates of larger eukaryotic phytoplankton, highest for diatoms, exceeded those of PRO and SYN. Dilution estimates of growth were consistent with inferred rates from ^{14}C uptake and autotroph carbon.
- Nitrate uptake was associated with the production of larger phytoplankton and gave *f*-ratios (0.36) six-times higher than the export ratios from sediment traps and thorium (Stukel *et al.*, 2016). Both nitrogen and phosphorus were preferentially remineralized from sinking particles above 90 m. High grazing rates and remineralization of fecal pellets in the euphotic zone (Stukel *et al.*, 2013) suggest that mesozooplankton play a key role in shunting new production to higher trophic levels rather than to vertical POM flux (Décima *et al.*, 2016; Stukel *et al.*, 2016).
- The shallow thermocline of the CRD significantly reduces $bSiO_2$ dissolution rates below the mixed layer, creating a strong silicate pump (Krause *et al.*, 2016). Diatoms contribute 3–13% to new production, and ~6% to C export. These results suggest substantial food-web transformation of diatom production in the euphotic zone, which enriches $bSiO_2$ in exported material.
- SYN, the dominant photosynthetic bacterium, contributed ~25% of phytoplankton carbon biomass, but disproportionately less to production and export (Stukel *et al.*, 2013; Landry *et al.*, 2016). High microzooplankton grazing of SYN indicated a production deficit. Export was mediated by intact cells in zooplankton fecal pellets.
- Mesozooplankton biomass was high (~5 g dry weight m^{-2}) and relatively uniform, whereas grazing impact (12–50% of Chl *a* day^{-1}) was variable, with lower rates in the central dome region (Décima *et al.*, 2016). Grazing variability was associated with zooplankton size structure and composition and with partitioning of primary production between pico-sized and larger phytoplankton. These results suggest community changes in water parcels advected away from the upwelling area.

- Distinct differences were found in abundances and vertical distributions of Eucalanoid copepods in the areas examined, with the coastal area supporting a more diverse assemblage, two-fold greater abundance in the central CRD dominated by *Eucalanus inermis* (Jackson and Smith, 2016). Depth distribution was narrow and closely associated with the shallow thermocline in the central CRD. There was no evidence of daily vertical migration in the central CRD, but *E. inermis* demonstrated vertical migration in nearshore sampling.
- Combined data support a balance of phytoplankton production and grazing by micro- and mesozooplankton (Landry *et al.*, 2016). Production estimates of $\sim$1 g C m^{-2} day^{-1} from three approaches exceeded published regional averages by 2–3-fold. Pico-sized cells accounted for 39% of production. Microzooplankton consumed all PRO and SYN and two-third of total production. Production and grazing turnover are comparable to or higher than estimates for the upwelling system in the eastern equatorial Pacific.

Controls on phytoplankton stocks and plankton production

Experimental studies of phytoplankton control mechanisms involved shipboard grow-out incubations of several days duration with presumed limiting elements (Zn, Fe and Si additions, relative to controls), short-term (24-h) *in situ* incubations that manipulated grazer concentrations and light, and indices of potential limitation of secondary producers. Two studies conducted grow-out experiments (Chappell *et al.*, 2016; Goes *et al.*, 2016). The former reports the first profiles of Zn for the CRD region, and the latter is distinguished by size-fraction analysis to resolve treatment differences on small and large phytoplankton. Baines *et al.* (Baines *et al.*, 2016b) determined cellular trace metal composition of various unicellular plankton to assess signs of Zn, Fe or Si limitation and to evaluate whether elemental composition of food could limit metazoan production. Gutiérrez-Rodríguez *et al.* (Gutiérrez-Rodríguez *et al.*, 2016) investigated responses of the subsurface phytoplankton community of the CRD to changes in light and temperature associated with vertical displacement of water masses, coupling *in situ* transplanted dilution experiments with flow cytometry and epifluorescence microscopy to assess different groups. These results are interpreted in comparison with grazer dilution experiments incubated at the depth of sample collection (Landry *et al.*, 2016; Selph *et al.*, 2016). Baines *et al.* (Baines *et al.*, 2016a) measured the tissue concentrations and ratios of C, N, P, Fe and Zn in size-fractionated zooplankton samples to determine possible requirements and to find indications of trace metal limitation. Significant results from these studies include the following:

- Zn was significantly depleted relative to P and Si in the CRD upper water column compared with other oceanic systems (Chappell *et al.*, 2016). Si was limiting in grow-out experiments, but Si additions with either Fe or Zn led to higher biomass than Si alone. These results suggest that the Zn depletion relative to P in upwelled waters may create conditions that favor phytoplankton, like SYN, with low Zn requirements.
- Size-fractionated measurements of Chl *a* accumulation in grow-out experiments indicated that Si concentrations are sub-optimal for phytoplankton growth and that Si and light co-limit nano- and micro-sized phytoplankton as well as picophytoplankton (SYN and picoeukaryotes) (Goes *et al.*, 2016). The latter are consistent with recent reports of Si accumulation in SYN (Baines *et al.*, 2012). Results suggest that nano- and microplankton are limited by Si and Fe, and picophytoplankton by Zn, Fe as well as Si.
- Single-cell elemental analysis showed that flagellates at some stations may have been Fe stressed (Baines *et al.* 2016*b*). Diatoms had higher Fe:C, and were poorly silicified. Flagellate Fe:C and Zn:C were low enough to be a poor food source for metazoan zooplankton. Low RNA:DNA ratios in zooplankton support this idea. Metazoans that exploit apparent Fe and Zn-rich species and vertical heterogeneity in trace metal content might however avoid mineral limitation.
- Growth rates of SYN and picoeukaryotes were positively correlated with light in transplant experiments, and grazing and growth rates remained closely coupled despite perturbation of the growth environment (Gutiérrez-Rodríguez *et al.*, 2016). In contrast, larger phytoplankton, mainly diatoms, increased more than 10-fold in shallower transplant incubations, indicating that light plays a significant co-limiting role in controlling microphytoplankton populations.
- The ratio of Zn:C in the smallest zooplankton size fractions was $\sim$10 μmol mol^{-1}, which is lower than any previously published observation, possibly indicating mineral limitation of smaller zooplankton (Baines *et al.*, 2016*a*). Zn:C increased 3- to 4-fold with size until it was near the median of previously published values at 40 μmol mol^{-1}. Fe:C in zooplankton was similar to previously reported values and decreased with size. However, high Fe:C in small size fractions seemed to have a lithogenic origin. When corrected for this lithogenic Fe, Fe:C was typically 20–30 μmol mol^{-1}.

Microbial diversity and biogeochemistry of the OMZ

While our cruise was not designed as a study of microbial diversity or OMZ biogeochemistry, it nonetheless provided an opportunity for some work in these areas to be done in conjunction with experimental studies in the upper water column. Kong *et al.* (Kong *et al.*, 2013) investigated anammox bacterial communities in the OMZ based on hydrazine oxidoreductase (hzo) genes and their protein transcripts (Clusters 1 and 2). Cheung *et al.* (Cheung *et al.*, 2016) report community structure of diazotrophs in the deep OMZ at 1000 m based on analysis for the *nifH* gene by 454-pyrosequencing. Buchwald *et al.* (Buchwald *et al.*, in revision) used nitrite and nitrate concentrations and natural abundance isotope profiles of $\delta^{15}N$ and $\delta^{18}O$ from the cruise, along with a novel 1D reaction diffusion model, to predict rate profiles for nitrate reduction, nitrite reduction and nitrite oxidation throughout the water column into the deep OMZ. Similarly, Vedamati (Vedamati, 2013) used the opportunity from cruise sampling to investigate Fe redox cycling in the OMZ. They identified pronounced maxima in Fe(II) coincident with the secondary nitrite maxima at ~350–400 m. This feature is found in other OMZs, but is much deeper underlying the CRD than elsewhere. Significant results of these studies are as follows:

- The anammox communities showed low diversity, with peak hzo gene abundance in the upper OMZs, associated with the nitrite peak (Kong *et al.*, 2013). Nitrite and oxygen may therefore co-limit anammox bacteria. A novel hzo cluster 2× clade was abundant and widely distributed. Both Cluster 1 and 2 anammox bacteria played active roles in the OMZ, with Cluster 1 abundance and transcriptional activity higher in free-living and particle-attached cells.
- The diazotroph community was more unique and diverse in the OMZ core (350–700 m) than in low-oxygen waters above and below (Cheung *et al.*, 2016). Methanotroph-like diazotrophs dominated in this depth strata, suggesting potential coupling of nitrogen cycle and methane in the deep OMZ.
- The maximum rate of nitrite oxidation (10 nM day^{-1}) occurs above and below the secondary nitrite maximum, and the maximum rate of nitrate reduction (25 nM day^{-1}) occurs just above the maximum rate of nitrite reduction (15 nM day^{-1}) at the top of the OMZ (Buchwald *et al.*, in revision). Model predictions of concomitant nitrite oxidation and reduction in the OMZ are supported by microbial gene abundance profiles and rate incubations. These results suggest dynamic nitrite cycling in the OMZ, with implications for distributions of marine nitrifiers and interpretations of natural abundances of N and O isotopes.

SUMMARY

Despite its unexpected and opportunistic beginning, the FLUZiE project came together well to address many areas that were poorly understood about the CRD region. The resulting dataset is unprecedented with regard to the number of plankton community biomass and rate properties measured, the consistency of sampling strategy and the integration of stock, rate and experimental studies for the upper water column. The results confirm the importance of picophytoplankton biomass and production and the low contribution of diatoms, one of the region's unique characteristics as an upwelling center. They also show high zooplankton biomass, double that measured in the equatorial Pacific, despite similar phytoplankton production, which we found to be two to three times the average reported from previous shipboard measurements in the Papagayo subregion (Pennington *et al.*, 2006). While high zooplankton biomass in picophytoplankton-dominated waters may seem incongruous, we observed that the productivity of larger phytoplankton was disproportionate to their biomass and that food resources were concentrated in a shallow euphotic zone (e.g. less than half the depth of equatorial waters), which may allow more efficient feeding and growth of mesozooplankton. Mesozooplankton grazing was seen to be variable in the region and at least partially explained by variations in the partitioning of productivity between small and large cells in waters from different areas in and out of the central dome. An efficient Si pump, explained by low dissolution in the shallow cold thermocline, is consistent with reports of high bSi flux at depth, although it is not entirely clear that they are directly connected, or entirely due to diatoms. This is also the mechanism underlying a consistent result, limitation or co-limitation by silicic acid, from the experimental studies conducted during the cruise on (micro-)nutrient regulation of phytoplankton. We also report here the first profiles of Zn from the region, and Zn's low near-surface concentrations relative to P and Si, which could be one of the factors selecting for high concentrations of picophytoplankton, like SYN, with low Zn requirements.

While the results from this project have yielded some significant advances in understanding the structure and dynamics of plankton communities in the CRD region, it also has highlighted areas that would benefit from additional focused study in the future. One general area is the need to examine structure and process relationships

under normal or highly active conditions of CRD surface Chl *a* expression, to understand the range of system variability in production and dynamics, as well as the true contrasts between conditions in and out of the central dome region. It is clear that 2010 was an unusually suppressed year for the dome (Fig. 3), which makes the relatively high measured production rates that much more impressive and likely still conservative. At the same time, we also sampled concentrations of SYN almost an order of magnitude less than observed on previous CRD cruises; thus, there may be strong enhancements in picophytoplankton dominance and associated nutrient and trace element effects under more active upwelling conditions.

Results from this study also emphasize that much more needs to be learned about the rates and mechanisms that link upper water-column processes with export and differential transport/remineralization of material through the upper OMZ. We found a substantial discrepancy, for example, between measurements of nitrate uptake (new production) and nitrogen export, which could suggest either substantial lateral export of an unmeasured pool (e.g. dissolved organic nitrogen) or potential methodological issues in the measurements. The mechanisms that lead to a high rate of loss/remineralization of fecal material within the euphotic zone, with high recycling of N and P, need to be reconciled with efficient vertical transport of Si and Zn. Given high concentrations of SYN, which have measureable Si contents, and low stocks of diatoms, the partitioning of bSi between small and large phytoplankton, and other silicifying organisms like radiolarians beneath the euphotic zone, also requires more rigorous examination, including resolution of size-fractioned silicate uptake and kinetics. Certainly not last, but sufficient for this brief overview of future challenges, the region needs a focused research effort to resolve the differential effects of the various macro-nutrient and trace elements (Si, Co, Fe, Zn) that have now been separately hypothesized to explain unique characteristics of the CRD planktology. Our cruise results illustrate the valued added from detailed trophic and ecological studies done in conjunction with biogeochemical investigations, the underlying theme of the IMBER Program (Integrated Marine Biogeochemistry and Ecosystem Research). It is clear that biogeochemistry and plankton dynamics are very closely linked in the CRD, and that neither can be clearly understood without attention to the other.

SUPPLEMENTARY DATA

Supplementary data can be found online at http://plankt.oxfordjournals.org.

DATA ARCHIVING

The Cruise Report, data and metadata for this project are available through the Biological and Chemical Oceanography Data Management Office under the project title "Costa Rica Dome FLUx and Zinc Experiments" (http://www.bco-dmo.org/project/515387).

ACKNOWLEDGEMENTS

We gratefully acknowledge the professionalism and numerous accommodations, large and small, of Captain Chris Curl, the R/V *Melville* crew and resident technicians that greatly facilitated the cruise sampling and experimental programs. Rick Lumpkin of NOAA, AOML provided the WMO drifters. We also thank the many colleagues, post docs, students and technicians who contributed to the shipboard collections, post-cruise analyses and data presentations: Sharon Smith, Karen Selph, Stephen Baines, Dreux Chappell, Eric Firing, Jules Hummon, Andrés Gutiérrez-Rodríguez, Takafumi Kataoka, Mike Stukel, Moira Décima, Darcy Taniguchi, Alexis Pasulka, Andrew Taylor, Jagruti Vedamati, Christina Bradley, Xi Chen, Matthew Bruno, Melanie Jackson, Daniel Wick, John Wukuluk, Kate Tsyrklevich, Alison Brandeis, Heather Cyr, Kelly Keebler and Jessica Tsay.

FUNDING

This component of the CRD Flux and Zinc Experiments study was supported by U. S. National Science Foundation grants OCE-0826626 to M.R.L., -0825767 to J.I.G. and -0826027 to J.W.M.

REFERENCES

Baines, S. B., Chen, X., Twining, B. S., Fisher, N. S. and Landry, M. R. (2016a) Factors affecting Fe and Zn contents of mesozooplankton from the Costa Rican Upwelling Dome. *J. Plankton Res.*, **38**, 331–347.

Baines, S. B., Chen, X., Vogt, S., Fisher, N. S., Fisher, N. S., Twining, B. S. and Landry, M. R. (2016b) Microplankton trace element contents: implications for mineral limitation of mesozooplankton in an HNLC area. *J. Plankton Res.*, **38**, 256–270.

Baines, S. B., Twining, B. S., Brzezinski, M. A., Krause, J. W., Vogt, S., Assael, D. and McDaniel, H. (2012) Significant silicon accumulation by marine picocyanobacteria. *Nat. Geosci.*, **5**, 886–891.

Beers, J. R. and Stewart, G. L. (1971) Micro-zooplankters in the plankton communities of the upper waters of the eastern tropical Pacific. *Deep-Sea Res.*, **18**, 861–883.

Buchwald, C., Santoro, A. E., Stanley, R. H. R. and Casciotti, K. L. (in review) Nitrogen cycling in the secondary nitrite maximum in the Costa Rica Upwelling Dome". *Global Biogeochem. Cycle.*

Chappell, P. D., Vedamati, J., Selph, K. E., Cyr, H. A., Jenkins, B. D., Landry, M. R. and Moffett, J. W. (2016) Preferential depletion of zinc within Costa Rica Upwelling Dome creates conditions for zinc co-limitation of primary production. *J. Plankton Res.*, **38**, 244–255.

Cheung, S., Xia, X., Guo, C., Tan, S. and Liu, H. (2016) Diazotroph community structure in the deep oxygen minimum zone of the Costa Rica Dome. *J. Plankton Res.*, **38**, 380–391.

Crosby, D. S., Breaker, L. C. and Gemmill, W. H. (1993) A proposed definition for vector correlation in geophysics: theory and application. *J. Atmos. Ocean. Tech.*, **10**, 355–367.

Décima, M., Landry, M. R., Stukel, M. R., Lopez-Lopez, L. and Krause, J. W. (2016) Mesozooplankton biomass and grazing in the Costa Rica Dome: amplifying variability through the plankton food web. *J. Plankton Res.*, **38**, 317–330.

d'Ovidio, F., De Monte, S., Alvain, S., Dandonneau, Y. and Lévy, M. (2010) Fluid dynamical niches of phytoplankton types. *Proc. Natl Acad. Sci. USA*, **107**, 18366–18370.

Fiedler, P. C. (2002) The annual cycle and biological effects of the Costa Rica Dome. *Deep-Sea Res. I*, **49**, 321–338.

Fiedler, P. C. and Talley, L. D. (2006) Hydrography of the eastern tropical Pacific: a review. *Progr. Oceanogr.*, **69**, 143–180.

Firing, E. and Hummon, J. M. (2010) Shipboard ADCP measurements. The GO-SHIP Repeat Hydrography Manual: A Collection of Expert Reports and Guidelines, IOCCP Rep. 14, ICPO Publ. Ser, 134.

Franck, V. M., Bruland, K. W., Hutchins, D. A. and Brzezinski, M. (2003) Iron and zinc effects on silicic acid and nitrate uptake kinetics in three high-nutrient, low-chlorophyll (HNLC) regions. *Mar. Ecol. Prog Ser.*, **252**, 15–33.

Freibott, A., Taylor, A. G., Selph, K. E., Liu, H., Zhang, W. and Landry, M. R. (2016) Biomass and composition of protistan grazers and heterotrophic bacteria in the Costa Rica Dome during summer 2010. *J. Plankton Res.*, **38**, 230–243.

Gill, A. E. (1982) *Atmosphere-ocean Dynamics*, Vol. 30. Academic Press, San Diego, CA.

Goericke, R. (2002) Top-down control of phytoplankton biomass and community structure in the monsoonal Arabian Sea. *Limnol. Oceanogr.*, **47**, 1307–1323.

Goes, J. I., do Rosario Gomes, H., Selph, K. E. and Landry, M. R. (2016) Biological response of Costa Rica Dome to light, silicic acid and trace metals. *J. Plankton Res.*, **38**, 290–304.

Gutiérrez-Rodríguez, A., Selph, K. E. and Landry, M. R. (2016) Phytoplankton growth and microzooplankton grazing dynamics across vertical environmental gradients determined by transplant *in situ* dilution experiments. *J. Plankton Res.*, **38**, 271–289.

Gutiérrez-Rodríguez, A., Slack, G., Daniels, E. F., Selph, K. E., Palenik, B. and Landry, M. R. (2014) Fine spatial structure of genetically distinct picocyanobacterial populations across environmental gradients in the Costa Rica Dome. *Limnol. Oceanogr.*, **59**, 705–723.

Hofmann, E. E., Busalacchi, A. J. and O'Brien, J. J. (1981) Wind generation of the Costa Rica dome. *Science*, **214**, 552–554.

Jackson, M. L. and Smith, S. L. (2016) Vertical distribution of Eucalanoid copepods within the Costa Rica Dome area of the Eastern Tropical Pacific. *J. Plankton Res.*, **38**, 305–316.

Kessler, W. S. (2006) The circulation of the eastern tropical Pacific: a review. *Prog Oceanogr.*, **69**, 181–217.

Kong, L., Jing, J., Kataoka, T., Buchwald, C. and Liu, H. (2013) Diversity and spatial distribution of hydrazine oxidoreductase (hzo) gene in the oxygen minimum zone off Costa Rica. *PLoS ONE*, **8**, e78275.

Krause, J. W., Stukel, M. R., Taylor, A. G., Taniguchi, D. A., De Verneil, A. and Landry, M. R. (2016) Net biogenic silica production and the contribution of diatoms to new production and organic matter export in the Costa Rica Dome ecosystem. *J. Plankton Res.*, **38**, 216–229.

LaCasce, J. H. (2008) Statistics from Lagrangian observations. *Prog. Oceanogr.*, **77**, 1–29.

Landry, M. R., Barber, R. T., Bidigare, R. R., Chai, F., Coale, K. H., Dam, H. G., Lewis, M. R., Lindley, S. T. *et al.* (1997) Iron and grazing constraints on primary production in the central equatorial Pacific: an EqPac synthesis. *Limnol. Oceanogr.*, **42**, 405–418.

Landry, M. R., Constantinou, J., Latasa, M., Brown, S. L., Bidigare, R. R. and Ondrusek, M. E. (2000) Biological response to iron fertilization in the eastern equatorial Pacific (IronEx II). III. Dynamics of phytoplankton growth and microzooplankton grazing. *Mar. Ecol. Prog. Ser.*, **201**, 57–72.

Landry, M. R. and Kirchman, D. L. (2002) Microbial community structure and variability in the tropical Pacific. *Deep-Sea Res. II*, **49**, 2669–2693.

Landry, M. R., Ohman, M. D., Goericke, R., Stukel, M. R. and Tsyrkevich, K. (2009) Lagrangian studies of phytoplankton growth and grazing relationships in a coastal upwelling ecosystem off Southern California. *Prog Oceanogr.*, **83**, 208–216.

Landry, M. R., Selph, K. E., Decima, M., Gutiérrez-Rodríguez, A., Stukel, M. R., Taylor, A. G. and Pasulka, A. L. (2016) Phytoplankton production and grazing balances in the Costa Rica Dome. *J. Plankton Res.*, **38**, 366–379.

Landry, M. R., Selph, K. E., Taylor, A. G., Décima, M., Balch, W. M. and Bidigare, R. R. (2011) Phytoplankton growth, grazing and production balances in the HNLC equatorial Pacific. *Deep-Sea Res. II*, **58**, 524–535.

Li, W. K. W., Subba Rao, D. V., Harrison, W. G., Smith, J. C., Cullen, J. J., Irwin, B. and Platt, T. (1983) Autotrophic picoplankton in the tropical ocean. *Science*, **219**, 292–295.

Longhurst, A. R. (1976) Interactions between zooplankton and phytoplankton profiles in the eastern tropical Pacific Ocean. *Deep-Sea Res.*, **23**, 729–754.

Love, C. M. (ed.) (1972–1978) *EASTROPAC Atlas*, vols. 1–11. National Marine Fisheries Service, Washington.

Naqvi, S. W. A., Moffett, J. W., Gauns, M. U., Narvekar, P. V., Pratihary, A. K., Naik, H., Shenoy, D. M., Jayakumar, D. A. *et al.* (2010) The Arabian Sea as a high-nutrient, low-chlorophyll region during the late Southwest Monsoon. *Biogeosciences*, **7**, 2091–2100.

Owen, R. W. and Zeitzschel, B. (1970) Phytoplankton production: seasonal change in the oceanic eastern tropical Pacific. *Mar. Biol.*, **7**, 32–36.

Pennington, J. T., Mahoney, K. L., Kuwahara, V. S., Kolber, D. D., Calienes, R. and Chavez, F. P. (2006) Primary production in the eastern tropical Pacific: a review. *Prog Oceanogr.*, **69**, 285–317.

Saito, M. A., Rocap, G. and Moffett, J. W. (2005) Production of cobalt binding ligands in a *Synechococcus* feature at the Costa Rica upwelling dome. *Limnol. Oceanogr.*, **50**, 279–290.

Saito, M. A., Sigman, D. M. and Morel, F. M. M. (2003) The bioinorganic chemistry of the ancient ocean: the co-evolution of cyanobacterial metal requirements and biogeochemical cycles at the Archean-Proterozoic boundary? *Inorg Chim. Acta*, **356**, 308–318.

Selph, K. E., Landry, M. R., Taylor, A. G., Gutiérrez-Rodríguez, A., Stukel, M. R., Wokuluk, J. and Pasulka, A. (2016) Phytoplankton production and taxon-specific growth rates in the Costa Rica Dome. *J. Plankton Res.*, **38**, 199–215.

Smith, S. L. (2001) Understanding the Arabian Sea: reflections on the 1994–1996 Arabian Sea Expedition. *Deep-Sea Res. II*, **48**, 1385–1402.

Stukel, M. R., Benitez-Nelson, C. R., Décima, M., Taylor, A. G., Buchwald, C. and Landry, M. R. (2016) The biological pump in the Costa Rica Dome: an open ocean upwelling system with high new production and low export. *J. Plankton Res.*, **38**, 348–365.

Stukel, M. R., Décima, M., Selph, K. E., Taniguchi, D. A. A. and Landry, M. R. (2013) The role of Synechococcus in vertical flux in the Costa Rica upwelling dome. *Prog. Oceanogr.*, **112–113**, 49–59.

Taylor, A. G., Landry, M. R., Freibott, A., Selph, K. E. and Gutiérrez-Rodríguez, A. (2016) Patterns of microbial community biomass, composition and HPLC diagnostic pigments in the Costa Rica upwelling dome. *J. Plankton Res.*, **38**, 183–198.

Umatani, S. and Yamagata, T. (1991) Response of the eastern tropical Pacific to meridional migration of the ITCZ: the generation of the Costa Rica Dome. *J. Phys. Oceanogr.*, **21**, 346–363.

Vedamati, J. (2013) Comparative behavior and distribution of biologically relevant trace metals, iron, manganese and copper in four representative oxygen deficient regimes of the world's oceans. Ph.D. (Ocean Sciences) dissertation, Univ. Southern California, 236pp.

Wiggert, J. D., Murtugudde, R. G. and Christian, J. R. (2006) Annual ecosystem variability in the tropical Indian Ocean: Results of a coupled bio-physical ocean general circulation model. *Deep-Sea Res. II*, **53**, 644–676.

Wyrtki, K. (1964) Upwelling in the Costa Rica dome. *Fish. Bull.*, **63**, 355–372.